Management and control of short-term energy storage systems in electric ship

Hardan, Faysal; Tricoli, Pietro

Management and control of short-term energy storage systems in electric ship

F. Hardan , P. Tricoli
Department of Electronic, Electrical and Systems Engineering
School of Engineering
University of Birmingham, Birmingham, B15 2TT, UK

***Abstract*—This paper proposes and studies a DC power system with SMES and ultracapacitor energy storage modules and their control system for an electric ship. The system allows the storage modules to primarily regulate the voltage of the ship DC switchboard against high fluctuation caused by any transient loads onboard. As such, the ship battery as prime mover only provides the average component of the total dynamic power, which can be far below the peak power supplied frequently to the load. This procedure would eventually lead to extending the lifespan of the battery and to the deferral of its costly replacement. The paper also covers comparison of the power system efficiency when connecting the energy storage modules. The dynamic results, obtained via real-time hardware-in-the-loop simulation and control implementation, have validated the concept, and helped to assess the design characteristics and system performance.**

***Index Terms*—DC power system, ultracapacitor, SMES, power electronic converter, propulsion power, control system, ship, battery lifespan, hardware-in-the-loop simulation.**

I. INTRODUCTION

The number of electric ships is expected to increase considerably in the coming years in response to climate crisis and policies to decarbonise and electrify maritime transport systems. As such, the demand for ship batteries will grow by time around technologies that provide higher energy density for longer travelling range at lower cost. However, batteries have limited charging/discharging cycles and are expensive to replace at their end-of-life service. Therefore, any attempts that lead to prolonging their service life are highly desirable, such as increasing the efficiency of the ship's power converters and incorporating short-term energy storage systems (ESSs). These systems have much higher number of charging cycles and can be charged or discharged rapidly to handle peak and transient power requirements of the ship's propulsion units. In this context, the paper reports on the application of short-term ESSs, namely ultracapacitor energy storage (UCES) and superconducting magnetic energy storage (SMES) systems and their coordinated control and operation in a battery-powered electric ship. Current advancement in ultracapacitor (UC) technology has led to increasing energy densities, with current figures above 4.3Wh/L, and power densities of about 15kW/L [1]. It has been also reported that a compact super-conducting magnet (SM) technology produced by Si microfabrication technology can achieve energy density in the range of 1Wh/L or more [2]. To integrate the ESSs into the ship/vessel power system, different DC/AC microgrid architectures have been studied, [3]-[9]. A DC power system that connects the power-electronic (PE) converters of the UCES and SMES systems were studied and designed in addition to the control structure of the ship power system. The process also covered design and validation of the ESS local power controllers for proof-of-concept and assessment through real-time hardware-in-the-loop (HiL) simulation with DSP-controller implementation. The results of the dynamic power tests, obtained via the HiL and DSP implementation, conformed to those results obtained through modelling and simulation of the integrated vessel's power system. Both groups of results demonstrated how the short-term ESSs handled the peak and dynamic power efficiently whilst leaving the battery only involved in delivering an averaged slow-changing power to the load. As such, the battery's internal ohmic/heat losses, which are proportional to its current squared, will be considerably decreased when its current peaks are shaved. Reducing these losses, which can increase the internal temperature, would help to maintain the battery performance and to extend its lifespan [10]. Also, the paper illustrates how the UCES system enhanced the overall efficiency of the DC power system. The paper is organised in the following manner. Section II details the HiL simulated power system onboard the ship, including the DC switchboard, the UCES and SMES systems, as well as their PE converters. In section III, the proposed concept of the control system is covered with system modelling and analysis. Section IV compares the total efficiencies of the ship power system using the ESSs with typical Si and wide-bandgap (SiC) power-electronic devices or modules. The real-time HiL system simulation of the complete power and the obtained results are discussed in section V.

II. THE SHIP POWER SYSTEM ARCHITECTURE

The selected architecture of the DC power system that can accommodate the ESSs is represented by a simplified circuit diagram of the vessel's DC switchboard in Fig. 1, which does not include any redundant DC switchboards. The top-left part of the diagram represents the battery pack and its half-bridge PE converter which can be based on either Si IGBT modules or SiC MOSFET devices. The converter is connected to the DC-bus of the microgrid which is supported by the electrolytic capacitor C_{dc}. The

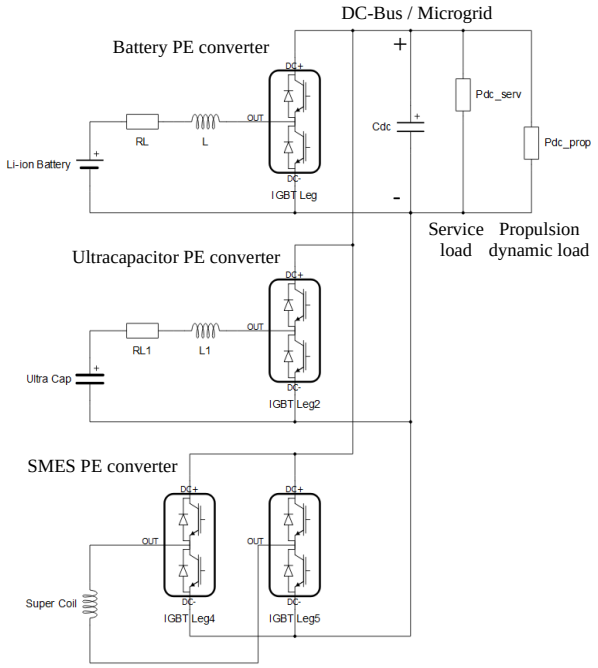

Fig.1. A simplified version of the vessel's DC switchboard (without connection of redundancy switchboard) including the ESS components and their power-electronic converters

middle part represents the UCES system which has the same structure as the top-left part, and it is also connected in parallel to the DC-bus. The lower part of the circuit diagram illustrates the structure of the SMES system which utilises a full-bridge PE converter to circulate the SM current through the DC-bus capacitor. The electric resistance R_{dc_serv} and R_{dc_prop} represent the vessel's service and propulsion dynamic loads, respectively, which connect directly to the DC power system. The specifications and component parameters of the vessel's power system are summarized in Table I. Although the battery PE converter is designed to operate at 150kW maximum power for higher power margin, it will be intended to operate below 100kW most of the time. The power difference for the dynamic and peak power delivery will always be provided by the UCES and SMES systems. The values of the UC capacitance and the SM inductance were chosen to be similar and equal to 10F and 10H, respectively, for symmetry and simplicity of design, analysis, and comparison. Based on these values, each ESS can store energy up to 1.8MJ at 600V for the UC and at 600A for the SM. In the reported case-study in this paper, it was assumed that the average value of the internal ESR of the UC is around 80 $m\Omega$ which matches that of the most advanced UC module available commercially [11].

TABLE I. SPECIFICATIONS AND MAIN DESIGN PARAMETERS OF THE SHIP POWER SYSTEM

DC-bus	750V DC (can be expanded up to 1kV), 200kW, $\boldsymbol{C_{dc} = 40mF}$
Battery (Li-ion)	250Ah, 400V, 250A, 200kW (peak), 100kW (av)
UCES	C=10F, 100kW (nom), voltage range: 200V to 600V, max stored energy: 1.8MJ
SMES	L=10H, 100kW (nom), current range: 200A to 600A, max stored energy: 1.8MJ

III. THE CONCEPT OF THE CONTROL SYSTEM

The control system concept is mainly focussed around regulating the DC-bus voltage whilst supplying the DC current to the motor drives of the ship's propulsion system. However, withdrawing such current causes the DC-bus voltage to drop rapidly unless compensated. Therefore, the aim is to deliver the compensating current by controlling the UCES and SMES PE converters to react, within a suitable response-time, to any drop or rise in the DC voltage, as illustrated via the block diagram in Fig.2. This current flow in turn will cause changes in the stored energies of the UCES and SMES systems, demonstrated by changes in the UC voltage and SM current. The UC current demand i_{uc}^* is simply generated by multiplying the DC-bus voltage error by the voltage-droop gain G_{duc}, whilst the SM current demand i_{sm}^* is derived by multiplying the DC-bus voltage error by the relevant voltage-droop gain G_{dsm}. It is worth mentioning that the SMES output current to the DC-bus is controlled by modulating an SMES reference voltage v_{sm}^*, which can be derived by equating the SMES power at the coil side with the SMES power delivered to the DC-bus. The power losses of the SMES PE converter are neglected in this case for modelling and control purposes. As such, the reference voltage of the SMES system v_{sm}^*, pulse-width-modulated inside the SMES PE converter, can be derived as follows,

$$v_{sm}^* = \frac{i_{sm}^* \cdot V_{dc}}{I_{sm}} \tag{1}$$

i_{sm}^* is the demand for the average SMES current to the DC-bus, V_{dc} is the DC-bus voltage, and I_{sm} is the SMES coil current. All variables are indicated within the block diagram of the control system in Fig.2.

A. Representation of the stored-energy control-loops

To avoid depleting the charges of the UC and SM coil, an outer control-loop (represented by the lower part of the diagram) was integrated to the control system with very slow-response to bring back the stored energy in these storage components to its nominal/reference setting. The difference between the stored energy and its reference or nominal value is to be driven to zero by the re-charging controller. This in turn demands the battery PE converter to deliver a slow-changing current to the DC-bus, which eventually represents the load average current plus the required re-charging current. The representation of the stored-energy control-loops, in terms of the UC voltage and SM coil current, has been derived as follows. The ultracapacitor energy, as a function of its voltage V_{uc} can be defined as

$$E_{uc}(V_{uc}) = \frac{1}{2}\, C_{uc}\, V_{uc}^2 \tag{2}$$

C_{uc} is the capacitance of the UC. Linearizing this expression around the UC nominal voltage V_{ucn} gives

$$\begin{aligned} &E_{uc}(V_{uc}) \cong E_{ucn} + C_{uc}\, V_{ucn}\, (V_{uc} - V_{ucn}) \;\rightarrow \\ &E_{ucn} - E_{uc}(V_{uc}) \cong C_{uc}\, V_{ucn}\, (V_{ucn} - V_{uc}) \text{ , or} \\ &E_{rruc} \cong C_{uc}\, V_{ucn}\, (V_{uc}^* - V_{uc}) \\ &E_{rruc} = E_{ucn} - E_{uc}(V_{uc}) = E_{uc}^* - E_{uc}(V_{uc}) \end{aligned} \tag{3}$$

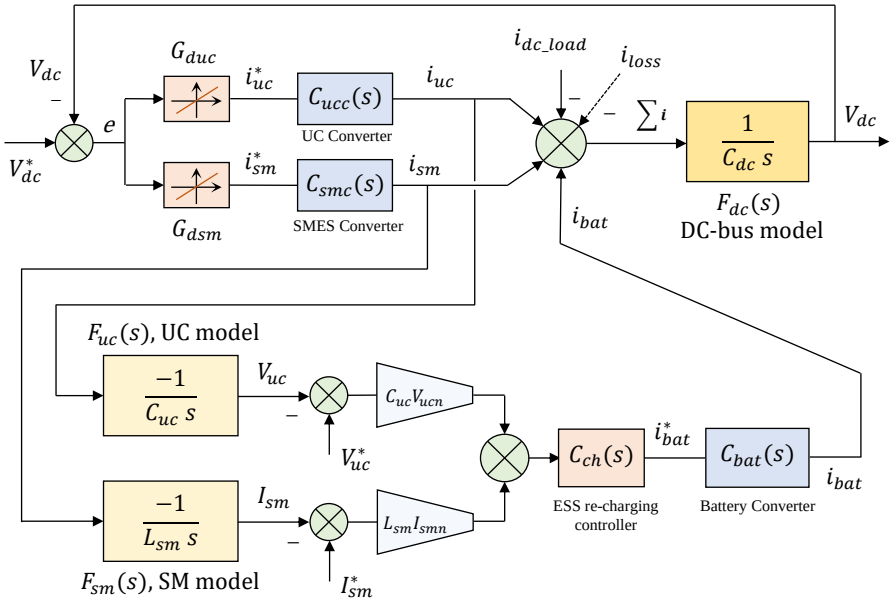

$$C_{bat}(s) = C_{ucc}(s) \cong 1/(1+\tau_{ucc}s)\ ;\ \tau_{ucc} \cong 2ms\ ,$$
$$C_{smc}(s) \cong 1/(1+\tau_{smc}s)\ ;\ \tau_{smc} \cong 1ms$$

Fig.2. A block-diagram representing the close-loop controller of the DC-bus voltage and the re-charting control loop for the UCES and SMES systems for linearized dynamic modelling, design, and analysis

where, the UC reference voltage is set to the UC nominal voltage for calculating the UC energy error E_{rruc}. Also, the stored energy in the SMES coil is a function of the coil current I_{sm} and can be expressed as

$$E_{sm}(I_{sm}) = \frac{1}{2}\, L_{sm}\, I_{sm}^2 \qquad (4)$$

L_{sm} is the SM coil inductance. Using the same linearization procedure around the nominal value of the coil current I_{smn}, the following approximate expression for the SMES energy error E_{rrsm} can also be derived,

$$E_{rrsm} \cong L_{sm}\, I_{smn}\, (I_{smn} - I_{sm})\ , \text{or}$$
$$E_{rrsm} \cong L_{sm}\, I_{smn}\, (I^*_{sm} - I_{sm}) \qquad (5)$$

when the reference of the SMES coil current is set to its nominal value. Equation (3) and (5) show that the stored-energy errors E_{rruc} , E_{rrsm} for the UCES and SMES systems can be replaced with the UC voltage and SM current errors multiplied by $C_{uc}\, V_{ucn}$ and $L_{sm}\, I_{smn}$, respectively. This procedure is demonstrated within the block diagram of the control system.

B. System modelling and analysis

To analyse the behaviour of the close-loop controlled system represented in Fig.2, a complete model in the s-domain was derived. The power losses of the DC-bus represented by the current i_{loss} were neglected in comparison with the DC-load current for analysis purposes. The time-constant of the battery and UCES PE converters τ_{ucc} was approximately assumed 2ms, whilst the time-constant of the SMES converter τ_{smc} was set to 1ms due to the higher response of the SMES converter. In this study, only proportional gains G_{duc} and G_{dsm} that are commonly called DC voltage-droop gains, were considered for DC-voltage control via the UCES and SMES, respectively. The adoption of PI controllers for this purpose may easily result in control saturation, oscillation, and system instability. In contrast, controllers with only proportional gains are simple and effective as far as they restrict the DC-voltage within the recommended limits. Based on the derived model, the transfer functions, which connect the DC-load current i_{dc_load} as input to the DC-bus voltage at different voltage-droop gains, were found and are given in the Appendix. It should be noted that in all cases the ESS re-charging controller is considered as simple proportional-integrator function with tuned and fixed gains (proportional gain $K_p = 0.0005$, integral gain $K_i = 0.000125$). Based on the model's transfer functions, the graphs in Fig.3 illustrate the step and frequency responses of the DC-bus voltage when the DC-load current is stepped up from 0 to its rated value. In Fig.3 (a), the step response demonstrates that at the initial instant (0s), when the DC-load current is suddenly changing to its rated value, the change in the DC-bus voltage is instantly dropped to -75V when setting the voltage-droop gains G_{duc} & G_{dsm} to 1.75. This change represents -10% of the nominal DC-bus voltage or its set point, which does not exceed the design and recommended-standard limits of ±10% [12] and [13]. The change becomes less as the DC-bus voltage-droop gain goes higher, e.g., it is reduced to the half when the gain is doubled in value, as illustrated by graphs 1, 2 and 3. In general, it can be realised that increasing the gains G_{duc} and G_{dsm}, will always result in more damped response and less fluctuation in the DC-bus voltage. The graphs in Fig.3 (b) illustrate the

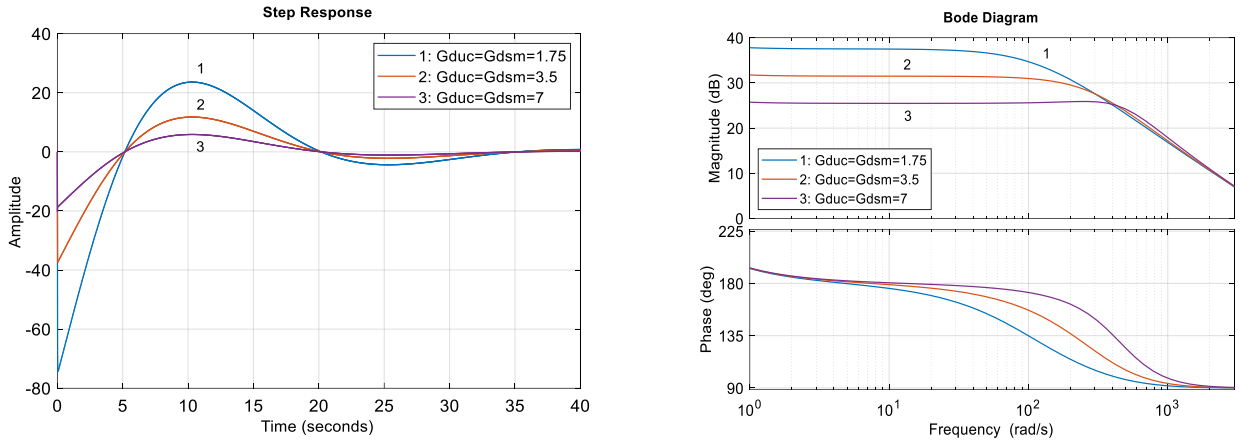

(a) (b)

Fig.3. (a): the step response of the DC-bus voltage when the DC-load current is stepped up from 0 to its rated level, (b): the corresponding frequency response

corresponding frequency response of the DC-bus voltage. They demonstrate how the control bandwidth increases when the voltage-droop gain becomes higher. For the cases relevant to graphs 1, 2, and 3, as the gain changes in the range from 1.75 to 7, the control bandwidth of the DC-bus voltage would approximately change within the range from 400 to 1000 rad/s.

IV. System Efficiency Using Different PE Technology

To assess the most suitable short-term ESS for integration into the vessel power system, a comparison in terms of power losses, efficiency, and the effect of each ESS on the total efficiency of the power system was carries out when relying on Si and SiC PE technologies. The considered assumptions and operational conditions for evaluating the losses and efficiencies with different cases of ESS operation are provided the Appendix. The comparison is summarized in Table II for five operational cases at which the vessel battery is delivering its nominal power of 100kW. It can be realised that when the UCES system is contributing 50kW power to the DC load (case 2), the total efficiency was increased by 0.3% when employing typical Si PE modules, and by 0.26% when utilizing typical SiC PE devices. However, a remarkable reduction in the total efficiency was noticed when the SMES system is invoked (cases 3, 4, 5) as it caused the total losses to increase by around 7kW when using the Si modules, and by 6kW when utilising the SiC devices.

V. Results and Discussion

To assess the performance and validate the design characteristics of the proposed power and control systems, the power components including the PE converters, as well as the control system were implemented within the hardware-in-the-loop platform and the TI Delfino DSP microcontroller board, respectively. The controllers of the control system, including the discrete-time model of the propulsion units, were all implemented and executed at 10kHz rate within the board. The measured outputs from the HiL platform, which represent physical voltage, current and power quantities, are all fed back to the controllers within the DSP microcontroller. Accordingly, the controllers' outputs are fed to the HiL platform from the DSP board through its D/A converters.

The graphs in Fig.4 illustrate the recorded voltage, current, and power variables with time, obtained through offline simulation of the power and control systems under a harsh operating scenario of the vessel's propulsion system. The load or propulsion power profile in this case is the result of sudden changes in the torque demands applied to the vessel's propulsion shafts for rapid acceptation/deceleration of the ship. System ratings and specifications were considered as given in Table I, and the

TABLE II. Efficiency summary table considering typical Si and SiC power electronic devices/modules

[kW] / Case	Battery system power	UCES system power	SMES system power	Case total power losses (with Si PE)	Case total power losses (with SiC PE)	Case total efficiency % (with Si PE)	Case total efficiency % (with SiC PE)
Case 1	100	n/a	n/a	5.085	4.56	94.9	95.44
Case 2	100	50	n/a	7.257	6.435	**95.2**	**95.7**
Case 3	100	n/a	50	12.055	10.143	91.96	93.24
Case 4	100	50	50	14.227	12.019	92.89	93.99
Case 5	100	0	0	12.545	10.646	87.5	89.36

n/a: not applicable – or when an ESS is disconnected

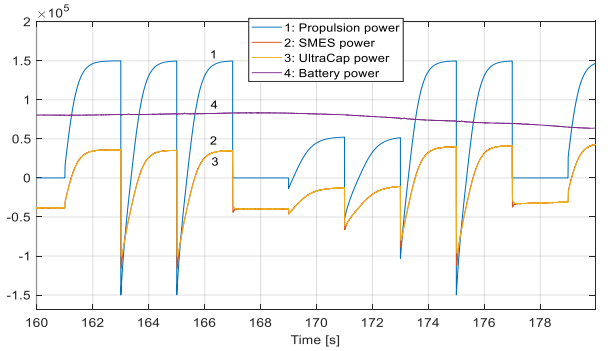

(a)

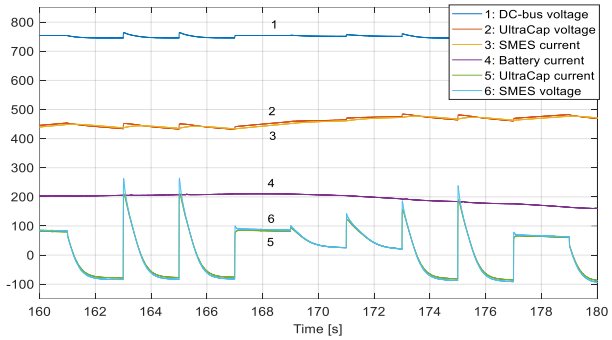

(b)

Fig.4. Dynamic power testing results obtained via offline system simulation; power is in (w), current is in (A), and voltage is in (V)

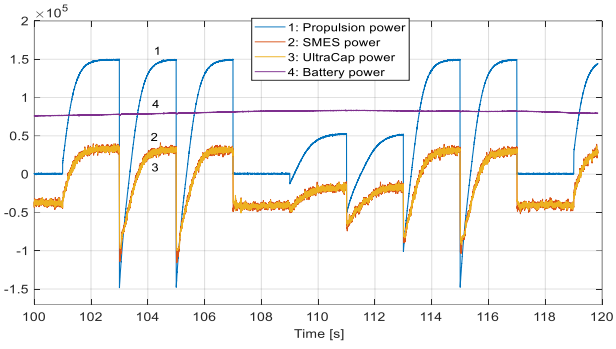

(a)

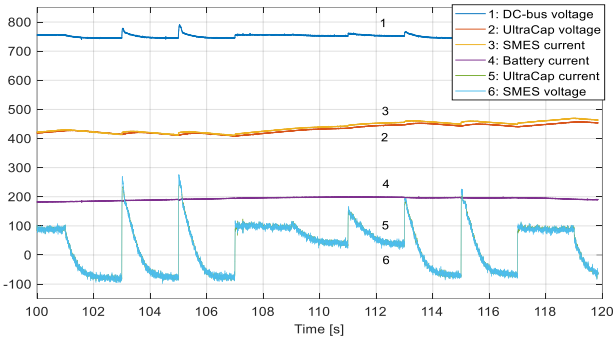

(b)

Fig.5. Dynamic power testing results obtained via HiL and DSP-controller implementation

DC-bus voltage-droop gains were assumed to be both equal to 3.5. As illustrated, the propulsion or the DC-load dynamic power is changing in the range between -150kW and +150kW. The negative power is the re-generative power due to the rotating mechanical inertia of the propulsion propellers, which was set to 10 kg.m^2. In group (a), it can be realised that the ultracapacitor and SMES power are changing dynamically with the same patterns as the propulsion load/power to compensate the difference between the load and the battery power. The latter is a slow-changing variable around its average value over a designed time-window of few minutes. The corresponding graphs of the recorded voltages of the DC-bus, ultracapacitor and SMES, as well as their currents and battery current, are all illustrated in graph (b). It is demonstrated how the DC-bus voltage fluctuation stayed within the recommended limits ±10, whilst the ultracapacitor storage voltage and SMES storage current are changing slowly as functions of the ultracapacitor and SMES power, respectively. The ultracapacitor current and SMES averaged voltage are both changing in the same pattern as their corresponding power, but in the opposite manner according to their assigned direction.

The results obtained through the real-time HiL simulation and implementation of the proposed control system, under the same conditions applied for the offline simulation, are given in Fig.5. The obtained graphs are in a strong agreement with the graphs of Fig.4, which also validate the design characteristics and objective of the power and control systems. The system performance demonstrated through the real-time HiL and control implementation and offline system simulation, are both matching the design specifications expected by the presented vessel's power system. For instance, the DC-bus voltage is always regulated around its set point 750V, whilst the ultracapacitor and SMES power are changing with high-response to any variation in the DC-bus voltage when the DC-load or propulsion power is changing rapidly. And the battery power, as can be realised, is changing slowly around its nominal value in response to the ESS re-charging controller.

VI. Conclusion

The paper presented an innovative ship power system, combining SMES and ultracapacitor energy storage modules, with associated control system for electric vessel. It was demonstrated through HiL simulation and DSP microcontroller implementation that the proposed power architecture and control concept are highly effective in neutralizing the effect of transient loads onboard the ship. It is also discussed, through efficiency analysis and comparison, how the ultracapacitor module alone increased the power system efficiency up to 0.3% with Si PE converter, and up to 0.26% when using converter with SiC PE modules.

Acknowledgment

The authors acknowledge the financial support received through the TRIG programme of the UK Department for Transport, project no. 1320-b; UKRI, project no. 1005639; and EU Horizon, grant agreement no. 101096831.

REFERENCES

[1] S. I. Wong, J. Sunarso, B. T. Wong, H. Lin, A. Y. Baohua Jia, "Towards enhanced energy density of graphene-based supercapacitors: Current status, approaches, and future directions", Journal of Power Sources, vol. 396, pp. 182-206, 2018, doi: 10.1016/j.jpowsour.2018.06.004.

[2] T. Motohiro, M. Sasaki, J. Noh, and O. Takai, "Estimation of the Electricity Storage Volume Density of Compact SMESs of a New Concept Based on Si Microfabrication Technologies," Magnetochemistry, vol. 7, no. 3, p. 44, Mar. 2021, doi: 10.3390/magnetochemistry7030044.

[3] Z. Jin, G. Sulligoi, R. Cuzner, L. Meng, J. C. Vasquez and J. M. Guerrero, "Next-Generation Shipboard DC Power System: Introduction Smart Grid and dc Microgrid Technologies into Maritime Electrical Netowrks," in IEEE Electrification Magazine, vol. 4, no. 2, pp. 45-57, June 2016, doi: 10.1109/MELE.2016.2544203.

[4] A. Shekhar, L. Ramírez-Elizondo and P. Bauer, "DC microgrid islands on ships," 2017 IEEE Second International Conference on DC Microgrids (ICDCM), Nuremburg, Germany, 2017, pp. 111-118, doi: 10.1109/ICDCM.2017.8001031.

[5] F.D. Kanellos, G.J. Tsekouras, J. Prousalidis, "Onboard DC grid employing smart grid technology: challenges, state of the art and future prospects", IET Electrical Systems in Transportation, vol. 5, no. 1, pp.1-11, 2015, doi: 10.1049/iet-est.2013.0056.

[6] L. Xu *et al*., "A Review of DC Shipboard Microgrids—Part I: Power Architectures, Energy Storage, and Power Converters," in *IEEE Transactions on Power Electronics*, vol. 37, no. 5, pp. 5155-5172, May 2022, doi: 10.1109/TPEL.2021.3128417.

[7] A. Accetta and M. Pucci, "Energy Management System in DC Micro-Grids of Smart Ships: Main Gen-Set Fuel Consumption Minimization and Fault Compensation," in IEEE Transactions on Industry Applications, vol. 55, no. 3, pp. 3097-3113, May-June 2019, doi: 10.1109/TIA.2019.2896532.

[8] X. Zhaoxia, Z. Tianli, L. Huaimin, J. M. Guerrero, C. -L. Su and J. C. Vásquez, "Coordinated Control of a Hybrid-Electric-Ferry Shipboard Microgrid," in IEEE Transactions on Transportation Electrification, vol. 5, no. 3, pp. 828-839, Sept. 2019, doi: 10.1109/TTE.2019.2928247.

[9] F. Hardan and R. Norman, "Provision of Synthetic Inertia via Energy Storage VSC for a Ship AC/DC Microgrid," The 10th International Conference on Power Electronics, Machines and Drives (PEMD 2020), Online Conference, 2020, pp. 556-562, doi: 10.1049/icp.2021.1088.

[10] F. Leng, C. Tan, M. Pecht, "Effect of Temperature on the Aging rate of Li Ion Battery Operating above Room Temperature", Scientific Report, vol. **5**, 12967, 2015, doi: 10.1038/srep12967.

[11] https://www.skeletontech.com/skelmod-102v-ultracapacitor-module - accessed on 06/09/2022

[12] Y. Khersonsky, "New IEEE standards for ships," 2011 IEEE Electric Ship Technologies Symposium, Alexandria, VA, USA, 2011, pp. 424-429, doi: 10.1109/ESTS.2011.5770909.

[13] D. Kumar and F. Zare, "A Comprehensive Review of Maritime Microgrids: System Architectures, Energy Efficiency, Power Quality, and Regulations," in IEEE Access, vol. 7, pp. 67249-67277, 2019, doi: 10.1109/ACCESS.2019.2917082.

APPENDIX

The transfer functions derived from the system model at different DC-bus voltage-droop gains:

1. For $G_{duc} = G_{dsm} = 5$, $F_{idc2vdc} = N(5)/D(5)$;
$N(5) = -(8 \times 10^{-13} s^7 + 2.8 \times 10^{-9} s^6 + 3.8 \times 10^{-6} s^5 + 0.0025\, s^4 + 0.8\, s^3 + 100\, s^2)$,
$D(5) = 3.2 \times 10^{-14} s^8 + 1.12 \times 10^{-10} s^7 + 1.541 \times 10^{-7} s^6 + 0.0001057\, s^5 + 0.03751\, s^4 + 6.312\, s^3 + 355.9\, s^2 + 80.09\, s + 20$.
2. For $G_{duc} = G_{dsm} = 10$, $F_{idc2vdc} = N(10)/D(10)$;
$N(10) = N(5)$,
$D(10) = 3.2 \times 10^{-14} s^8 + 1.12 \times 10^{-10} s^7 + 1.563 \times 10^{-7} s^6 + 0.0001114\, s^5 + 0.04302\, s^4 + 8.623\, s^3 + 711.8\, s^2 + 160.2\, s + 40$
3. For $G_{duc} = G_{dsm} = 20$, $F_{idc2vdc} = N(20)/D(20)$
$N(20) = N(5)$,
$D(20) = 3.2 \times 10^{-14} s^8 + 1.12 \times 10^{-10} s^7 + 1.605 \times 10^{-7} s^6 + 0.0001228\, s^5 + 0.05404\, s^4 + 13.25\, s^3 + 1424\, s^2 + 320.4\, s + 80$

THE CONSIDERED ASSUMPTIONS AND OPERATIONAL CONDITIONS FOR EVALUATING THE LOSSES AND EFFICIENCIES

	Battery (Li-ion)	**UCES**	**SMES**
Average power consumption of BMS/aux/cooling system	2kW	0.5kW	5kW
State of charge (SoC)	50%	50%	50%
Average internal resistance	20mΩ	80mΩ	0
PE converter topology	Half-bridge or one-leg (CCM operation)	Half-bridge or one-leg (CCM operation)	Full bridge (Unidirectional current op.)
Voltage and current ratings of the Si and SiC PE modules	1200V, 600A	1200V, 600A	1200V, 600A (for each PE leg)
Interfacing inductance, L, L_1	3mH, 10mΩ, ΔI_L=6.22A (peak-to-peak)	3mH, 10mΩ, ΔI_L=6.22A (peak-to-peak)	-